Progress In Electromagnetics Research, PIER 104, 297–311, 2010

PHASE DETECTION WITH SUB-NANOMETER SENSITIVITY USING POLARIZATION QUADRATURE ENCODING METHOD IN OPTICAL COHERENCE TOMOGRAPHY

W.-C. Kuo, C.-Y. Chuang, M.-Y. Chou, W.-H. Huang and S.-T. Cheng

Institute of Electro-optical Science and Technology
National Taiwan Normal University
Taipei 116, Taiwan

Abstract—This paper presents a phase-resolved optical coherence tomography (OCT) system that uses the polarization quadrature encoding method in a two-channel Mach-Zehnder interferometer. OCT is a powerful optical signal acquisition method that can capture depth-resolved micrometer-resolution images. In our method, a complex signal is optically generated, and its real and imaginary components are encoded in the orthogonal polarization states of one sample beam; absolute phase information can then be acquired instantaneously. Neither phase modulation nor numerical Fourier or Hilbert transformation to extract phase information is required, thereby decreasing data acquisition rates and processing time. We conducted signal post-processing to select data from the instabilities of reference scanning delay lines; the measured phase sensitivity was as low as 0.23°, and the corresponding path-difference resolution was 265 pm. A localized surface profile measurement of a chromium-coated layer deposited on a commercial resolution target surface was conducted. The results confirmed that successful images can be obtained even with very small optical path differences using the proposed method.

1. INTRODUCTION

Today, optical coherence tomography (OCT), which is based on low coherence interferometry, has become a powerful tool that can support non-contact high-speed tomographic imaging in transparent and turbid

Corresponding author: W.-C. Kuo (kwchuan@ntnu.edu.tw).

specimens [1]. By using this technique, the depth-resolved intensity of backreflected or backscattered optical radiation can be measured that micrometer-resolution images can be captured. Recently, OCT using various phase-sensitive detection techniques has been proposed to detect longitudinal displacement with pico-to-nanometer sensitivity; this makes it possible to measure layered structures in semiconductors and bio-tissue surfaces or cell responses to various stimuli [2–13].

Table 1 summarizes the typical approaches that have been developed to detect the phase information with OCT. For an optical system constructed in free space, a differential phase measurement setup using dual-channel polarization-sensitive OCT with a Wollaston prism was first reported by Hitzenberger in 1999 [2]. A Wollaston prism is placed at the focal point of a lens, where it splits the sample beam into two components. Here the phase difference between the two resulting focal spots is measured similarly to the phase retardation measurement caused by a birefringent sample in polarization-sensitive OCT. This idea was applied to a differential phase-contrast OCT (DPC-OCT) system by Sticker et al. in 2001 [3]. The difference between the two phase functions is obtained by using an OCT system with Hilbert transformation of the measured interference signals. This method has also been demonstrated using fiber-based OCT [4, 5]. However, the distance between the two focal spots of the sample beams which is separated by a Wollaston prism, limits the transversal resolution of the phase-contrast image. Sticker et al. presented a DPC-OCM setup as well in 2002 [6]. In this study, two sample beams with different FWHM diameters were coaxially combined and focused onto the sample. Such an arrangement permits the path-length difference

Table 1. Typical approaches for obtaining phase image. A: Wollaston prism; B: Coaxial beam; C: Optical referencing method; D: Spectrometer; E: Swept source; F: Buffered Fourier domain mode-locked laser.

		Free space	Fiber-based
Time-domain	A	C. K. Hitzenberger et al. [2] M. Sticker et al. [3]	D. P. Dav'e et al. [4] T. Akkin et al. [5]
	B	M. Sticker et al. [6]	
	C		F. Y. Christopher et al.[7]
Fourier-domain	D	A. H. Bachmann et al. [12]	M. A. Choma et al.[9] C. Joo et al.[11] J. Zhang et al.[13]
	E	M. V. Sarunic et al.[8]	M. A. Choma et al.[9]
	F		D. C. Adler et al.[10]

between the small spot beam and its surrounding to be measured and imaged-optical path length differences (OPL) as small as $\sim 2\,\text{nm}$ were reported. However, in DPC-OCM ghost images are generated, and moreover, the image contrast is dependent on the direction of beam separation; this restricts the applications of DPC-OCM.

Alternatively, Christopher et al. [7] proposed an optical referencing method wherein the light from the second output of the Michelson interferometer goes to a reference gap. In such a case, the phase change of the light reflected from a sample relative to a reflective surface above can be measured, but the setup incorporates both fiber and free-space elements and is complicated. Moreover, full interferometric signals, and not just envelopes are required to extract the phase term by using Hilbert transformation.

From 2005, various Fourier domain-OCT (FD-OCT) systems — using swept laser source [8, 9], buffered Fourier domain mode-locked lasers [10], or CCD array with a cooling system [9, 11–13] — have been proposed to extract depth-resolved intensity and phase information. In contrast to previous time domain-OCT (TD-OCT) phase measurement systems which involves the mechanical scanning of a reference mirror to perform A-scans in the time domain, the entire axial depth structure is acquired in parallel without involving any mechanical scanning of the reference mirror in FD-OCT systems enabling faster measurement and higher phase stability [14, 15]. Furthermore, FD-OCT systems can be constructed using a common-path configuration where the phase distribution of a sample referenced to the top surface of the coverslip is measured. Thus, longitudinal displacement detection at picometer-scale levels has been demonstrated using FD-OCT systems [9–11, 13].

In this study, we have proposed a phase-resolved OCT system that uses the polarization quadrature encoding method in a two-channel Mach-Zehnder interferometer. The complex signal is optically generated, and its real and imaginary components are encoded in the amplitude of the orthogonal polarization states of one sample beam; thus absolute phase information can be acquired instantaneously. Signal post-processing to select data from the instability of reference scanning delay lines is also introduced. The sensitivity of the longitudinal displacement detection at the picometer-scale level is achieved. The validity of the proposed method is demonstrated by performing experiments with a mirror for longitudinal displacement and the surface profile scanning of a chromium layer deposited on a commercial resolution target. The feasibility of the proposed method for samples with different reflectivities between orthogonally polarized light and whether the idea is applicable for FD-OCT system is also discussed.

2. THEORETICAL BACKGROUND AND EXPERIMENTAL SETUP

2.1. System Configuration

The experimental setup is shown in Fig. 1. A collimated beam from a superluminescent diode (SLD) centered at a wavelength λ_0 of 830 nm with a spectral bandwidth $\Delta\lambda$ of 16 nm was used as a low-coherence light source in a Mach-Zehnder interferometer. The axial resolution — $0.44\lambda_0^2/\Delta\lambda$ — was approximately 18.9 μm. After passing through a half-wave plate (HWP) and a polarizing beam splitter (PBS), the incident beam was divided into signal and reference beams. A quarter-wave plate (QWP) inserted into the sample arm was used to change the linear polarization state to circular polarized light. The 2 mm diameter beam was then focused by a 50 mm focal length lens (effective NA: 0.22) and scanned by a two-axis galvanoscanner mirror (XY-GM). A HWP was placed in the reference arm in order to rotate the *S*-polarized light into 45° linearly polarized state. A grating-based rapid-scanning optical delay (RSOD) line [16] using a 160 Hz resonant scanner (Z-GM), which creates separately controllable phase and group delays, was used in the reference arm for axial scanning. Finally, the

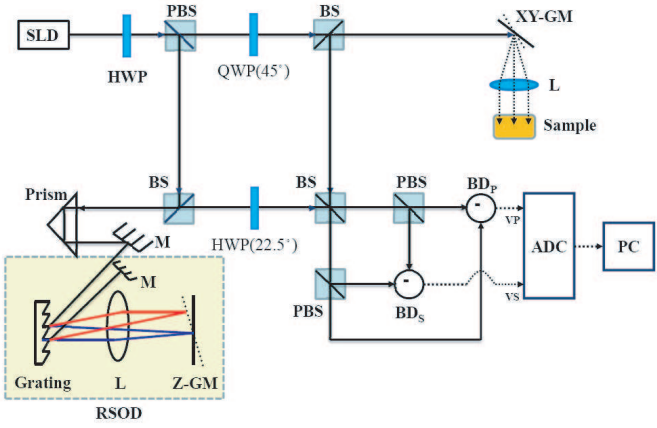

Figure 1. Schematic diagram of the system. SLD, superluminescent diode; HWP, half-wave plate; QWP, the quarter-wave plate; M, mirror; BS1-BS3, non-polarization beam splitters; PBS, polarized beam splitter; RSOD, rapid-scanning optical delay line; Z-GM and XY-GM, *z*-, *x*- and *y*-axis galvanoscanner mirrors; BD_P and BD_S, balanced detectors; ADC, analog-to-digital converter; and PC, personal computer.

light reflected from the sample recombined with the reflected reference beam, and both horizontal (P-wave) and vertical (S-wave) components were directed toward two balanced receivers (BD_P and BD_S) using two PBSs. Thus, the output signal current was not only double that from a single detector but also free from dc currents.

From the Jones matrix calculations, the interference signals V'_P and V'_S of the P-wave and S-wave components, respectively, are proportional to

$$V'_P(t) \propto A_p(t)\sin(\omega t + \phi), \tag{1}$$

and

$$V'_S(t) \propto A_S(t)\cos(\omega t + \phi), \tag{2}$$

respectively. Here $A_P(t)$ and $A_S(t)$ are the amplitudes of the P-wave and S-wave signals, respectively. In pure phase objects, $A_P(t) \approx A_S(t) = A(t)$. ϕ is the phase difference between the sample and reference arms in the P-wave and S-wave interference signals. When the source spectrum is centered on the pivoting axis of the galvo-mounted mirror, the RSOD generates only a group delay; no phase modulation is introduced during scanning [16]. Therefore, the two fully demodulated interferograms (i.e., without any fringe within their envelopes) have a 90° phase difference; this can be represented as follows:

$$V_P(t) \propto A(t)\sin(\phi), \tag{3}$$

$$V_S(t) \propto A(t)\cos(\phi). \tag{4}$$

$V_P(t)$ and $V_S(t)$ corresponds to the imaginary and real parts of an analytical signal, respectively. From the above equations, the optical phase fluctuation is converted into amplitude modulation and can be detected by using the conventional envelope detection technique. Thus, neither complete interferometric signals nor numerical Fourier or Hilbert transformation by using computers are required to extract phase information. Both the amplitude and phase tomographic images with a size of 1.5 mm × 3.5 mm can be acquired within 1 s by using

$$A(t) = \sqrt{V_P^2 + V_S^2}, \tag{5}$$

$$\phi = \angle\{V_S(t) + iV_P(t)\}. \tag{6}$$

Therefore, the difference in the OPL traversed by light between the sample and reference arms can be calculated from the phase term ϕ and the center wavelength of the source, λ_0, as follows:

$$OPL = \lambda_0\phi/4\pi. \tag{7}$$

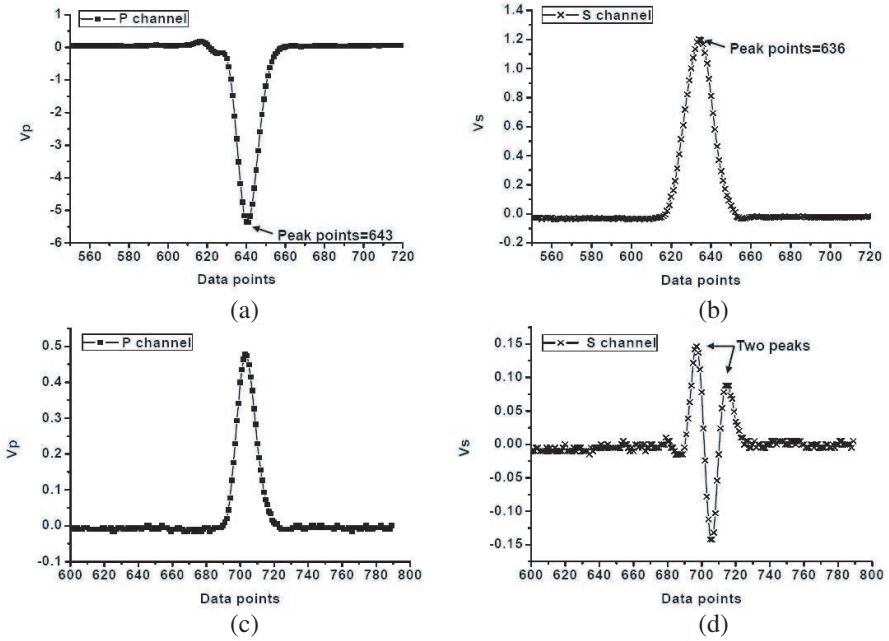

Figure 2. Representative curves of V_P (a) & (c) and V_S (b) & (d), which demonstrate instability due to the resonant mirror in RSOD.

2.2. Selection Algorithm

Figure 2 shows a representative curve that demonstrates instabilities as a result of the presence of a mechanical device (i.e., resonant mirror in RSOD); this might cause path mismatch during various measurements. As given in (3) and (4), the envelope amplitude is dependent on optical phase fluctuations. Hence, as shown in Figs. 2(a) and (b), the positions of the maximum peaks in both P-wave and S-wave are separated. Multiple peaks also existed in the S-wave interferometeric signal, as shown in Fig. 2(d). Therefore, we applied a selection algorithm to select data from the position of the maximum peaks in P-wave and S-wave separated by larger than 5 sampling points and when multiple peaks existed in either P-wave or S-wave signals.

3. RESULTS

Figure 3(a) shows a representative $V_S(t)$ which is plotted as a function of time. The measured axial resolution of the system was $\sim 19.3\,\mu m$. In this case, a fully demodulated interferogram is directly acquired by centering the source spectrum on the pivoting axis of the Z-GM, thus

the sampling rate needed is below 1 kHz. We also recorded $V'_S(t)$ signal as shown in Fig. 3(b) where the modulation frequency is set to 40 kHz by RSOD for comparison with our method. The sampling rate needs to be increased to 400 kHz so that the full interferometric signal was not distorted for phase information extraction.

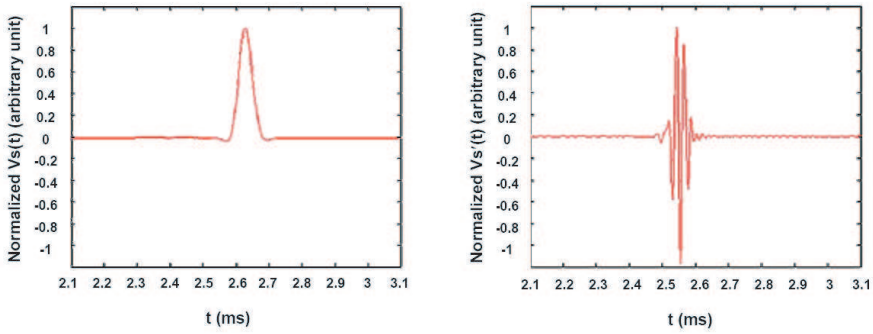

Figure 3. Interference S-wave signal recorded using a mirror as the sample in (a)without and (b) with phase modulation introduced during scanning.

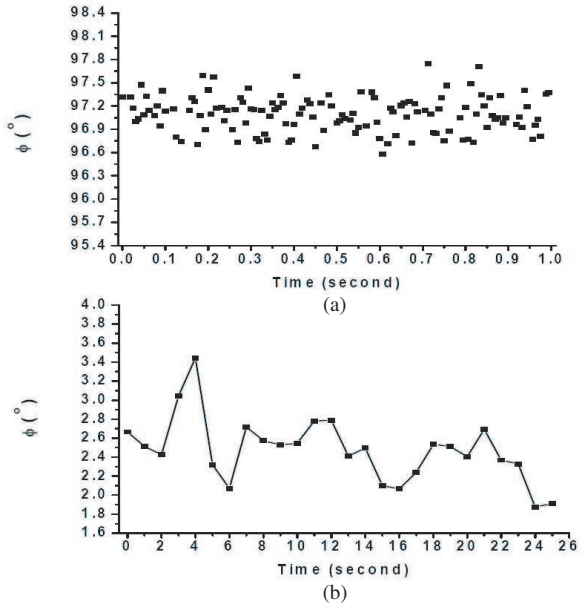

Figure 4. Temporal phase stability test of our proposed phase-resolved OCT system from a mirror surface within (a) 1-s and (b) 25-s measurement.

Figure 4 shows the results of the temporal stability test that is conducted by recording the ϕ signal from a mirror surface for a specified period of time. The phase sensitivity can be characterized by the variance of the phase, and is determined by the signal-to-noise ratio (SNR) of the phase measurement system [9, 11]. For a standard deviation (SD) of phase fluctuation of 0.23°, which directly yields the minimum detectable phase, calculated within 1 s of the measurement, the sensitivity of the longitudinal displacement was 265 pm, as shown in Fig. 4(a). For the measurement time of 25 s, as shown in Fig. 4(b), the sensitivity of longitudinal displacement was 392 pm. The measured SNR of our system was 36 dB, under which condition the theoretical sensitivity is 29.8 pm. The difference between the theoretical and measured sensitivities may be due to the influence of background disturbances such as vibrations as a result of the presence of a mechanical device (i.e., resonant mirror) during the measurements.

In order to verify the OPL (7) of the output signal in our system, the phase angle variation with the optical path difference produced by displacing the mirror longitudinally at 20 nm per step was measured using a PZT-controlled precision stage. The experimental results are shown in Fig. 5; the dynamic range of the measured phase ϕ is observed to be $-180° \sim 180°$, which corresponds to longitudinal displacement range of 430 nm. The measured data points are in good agreement with the expected values (solid line). However, the largest deviations occur when the measured phase ϕ is near 0°, ±90°, and ±180°. In these cases, the systematic deviations are probably caused by the detection channels — either P or S — obtaining very weak or no signal; this can be proved by (3) and (4).

The performance of the technique for quantitative phase imaging was tested with a commercial resolution target (Edmund: NBS 1963A); a chromium layer (thickness: $\sim$ 100 nm) was deposited on the target surface by evaporation. Fig. 6(a) shows a sketch of the sample arm configuration. A two-dimensional dataset of 100 adjacent axial scans was recorded within 1 s. Figs. 6(b) and 6(c) show the amplitude-contrast and phase-contrast images respectively. The amplitude-contrast image only shows the different reflectivities from the glass plate and the deposited chromium coating layer. However, from the phase-contrast image, a plot of the distribution of the differential phase between adjacent axial scans, $\Delta\phi$ along the surface of the object can be extracted as shown in Fig. 6(d). The change in $\Delta\phi$ is $\sim 93.4°$, which corresponds to step heights of $\sim$ 107 nm between the glass plate and chromium coating layer. This result confirms that the phase detection of the interference signal (e.g., Figs. 6(c) and 6(d)) allow

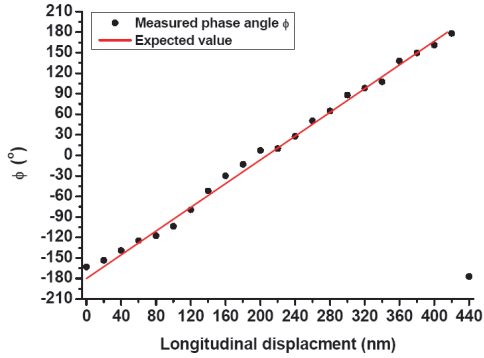

Figure 5. Dynamic range test of the proposed system by measuring the phase angle variations with the optical path difference produced by displacing a mirror longitudinally.

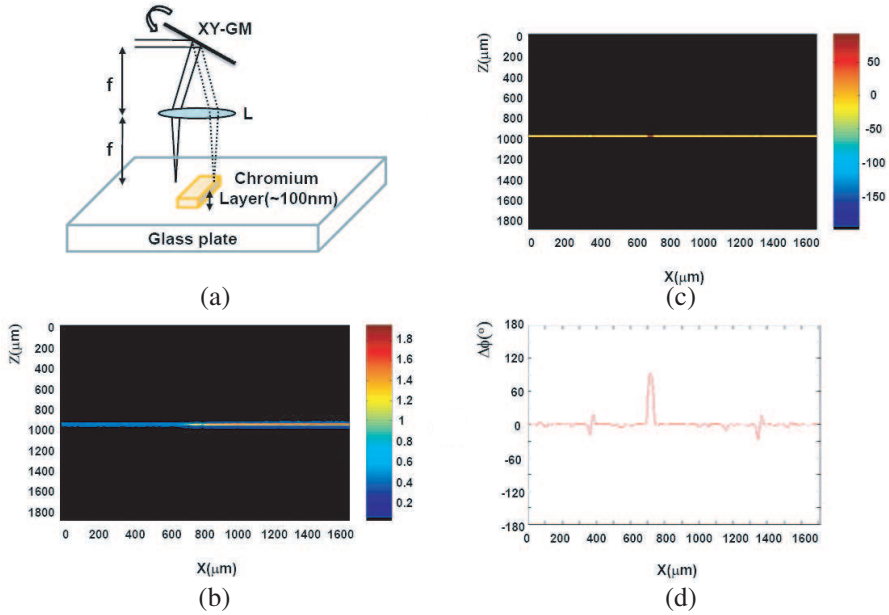

Figure 6. Images obtained with a commercial resolution target: (a) schematic diagram of the sample arm and phase object (chromium step), (b) amplitude-contrast image, (c) differential phase-contrast image, (d) $\Delta\phi$ distribution along the surface of phase object.

us to successfully image very small optical path differences that are invisible in amplitude-contrast images (e.g., Fig. 6(b)).

4. DISCUSSIONS AND CONCLUSION

In this paper, a novel phase-resolved optical low coherence interferometer that permits simultaneous amplitude- and phase-contrast imaging has been proposed. By using the interference between circular polarization and 45° linear polarization, a polarization quadrature encoding method was adopted in a two-channel Mach-Zehnder interferometer; this provides direct quantitative measurements of depth-resolved phases with sub-nanometer scale sensitivity in the reflection mode. Other analog phase decoding methods also apply both quadrature components of the complex interferometric signal, whereas phase shifting [17, 18] requires sequential measurements for a single image, which decrease the imaging speed, and a stable and carefully calibrated reference-arm setup. The phase shifting technique is also sensitive to any interferometer drifts between phase-shifted acquisitions. Synchronous detection [19], including lock-in detection and phase-locked loops, is not instantaneous and depends on the presence of an electronic carrier frequency. These methods lead to slower responses of the phase decoding.

In the proposed phase-resolved OCT configuration, a balanced detection technique removes the low-frequency background noise caused by different reflections of the RSOD during axial scanning and reduces the intensity noise [20, 21]. A signal post-processing is also used to select data from the instabilities caused by the reference scanning delay line. Thus, the measured phase sensitivity by this method is as low as 0.23 degree, which allows measurements of path-difference resolution of 265 pm in a displacement range of 430 nm. It is obvious that our method has better phase stability than the phase sensitivity experiments described in prior literatures [2–4, 6, 8, 12], which used either the Hilbert or Fourier transformation phase decoding method [22]. Besides, our technique which simply acquired optical phase fluctuation by using only the envelope decoding scheme has a reduction of data acquisition (e.g., at least 400 times less than the numerical phase decoding method as compared in Fig. 3).

When compared to the use of polarization-sensitive OCT [23–26] with polarization modulation for phase-sensitive detection [2] where the method measure the phase difference between the two separating and orthogonal-polarized sample beams in the same way as the phase retardation measurement in a birefringence sample. Our approach determines absolute phase difference between the sample

and the reference arm by using optically generated complex signal who's real and imaginary components are encoded in the amplitude of the orthogonal polarization states of one sample beam. Thus, no coaxial beams or separate beams are necessary, lateral resolution can be easily improved by using high-NA lenses and confocal detection of the backscattered light.

However, although a two-channel Mach-Zehnder interferometer was adopted in our proposed system which allows better polarization control, a drawback of our method is that for samples with different reflectivities in orthogonally polarized light, the assumption that $A_P(t) \approx A_S(t) = A(t)$ is no longer satisfied; this leads to the following phase angle measurement

$$\phi_N = \angle\{V_S(t) + iV_P(t)\} = \angle\{A_S(t)\cos(\phi) + iA_P(t)\sin(\phi)\}. \quad (8)$$

The systematic error in the OPL, ΔOPL, caused by the error between ϕ and ϕ_N is shown in Fig. 7 as a function of ϕ and A_S/A_P; A_S/A_P is the ratio between the amplitude of the S- and P-wave signals. It is obvious that either increasing or decreasing A_S/A_P causes the measured value of OPL to deviate from the actual value. For the sample with a constant reflectivity ratio between the amplitudes of the S-wave and P-wave signals, the distribution of the differential phases between the adjacent axial scans, $\Delta\phi$, along the surface of the object can be calculated. Thus the constant error in OPL is canceled out. Otherwise, a priori information about the distribution of A_S/A_P in the sample can be obtained by first offcentering the source spectrum on the mirror (i.e., Z-GM in Fig. 1) and then scanning the sample; the A_P and A_S terms in (1) and (2) can then be separately recorded and used to calibrate the phase measurement result by using a modification of (6) as follows:

$$\phi = \angle\left\{\frac{V_S(t)}{A_S(t)} + i\frac{V_P(t)}{A_P(t)}\right\}. \quad (9)$$

In this study, the validity and feasibility of this novel phase detection method is confirmed by performing experiments using a TD-OCT system. Although system with fiber-based implementation and the differential phase retrieval method may be used for improving the phase stability, our result shows performance an order of magnitude less than from those of the displacement sensitivity by FD SDPM [9], FDML-PSOCT [10] and SD-OCPM [11, 13]. We intend carrying out further experiments to evaluate the combination of this polarization quadrature encoding method with swept source- or CCD array-based FD-OCT system. From the Jones matrix calculations, the detected intensity using FD-OCT can be expressed by using a modification of

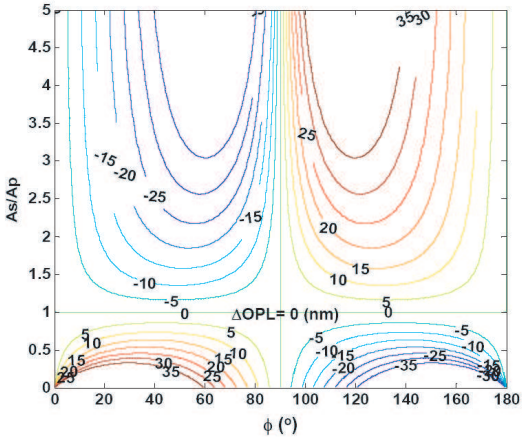

Figure 7. Contour plot of the systematic errors in measuring OPL, ΔOPL, as a function of actual phase angle ϕ, and the amplitude ratio A_S/A_P, caused by phase detection error in our proposed system when using samples with different reflectivities to S-wave and P-wave signals.

(1) and (2) as follows:

$$I_P(k) \propto 2S(k)\sqrt{R_R R}\sin(\phi), \tag{10}$$

and

$$I_S(k) \propto 2S(k)\sqrt{R_R R}\cos(\phi), \tag{11}$$

where k is the wavenumber; $S(k)$ is the spectral density of the light source; R_R and R are the reflectivities from the reference surface and the sample, respectively; and ϕ is the phase term.

Thus, the phase information can be retrieved by directly using the complex spectral signal as

$$\tilde{I}(k) = I_S(k) + iI_P(k) = 2S(k)\sqrt{R_R R}\exp[i\phi] \tag{12}$$

This is in contrast to the conventional phase-resolved FD-OCT system where the phase term is extracted by Fourier transformation of the detected spectral intensity and by tacking the argument of the transformed depth-resolved complex function. Since our approach is capable of obtaining phase information directly in spectral domain, thereby decreasing data processing time and the 2π ambiguity may also be corrected [13]. However, due to the extensive amount of information that needs to be addressed and further studies are required to support the suggestion, this will be the source of a separate publication.

ACKNOWLEDGMENT

This research was partially supported by National Science Council of Taiwan through Grant # NSC96-2628-M-003-001-MY3.

REFERENCES

1. Huang, D., E. A. Swanson, C. P. Lin, J. S. Schuman, W. G. Stinson, W. Chang, M. R. Hee, T. Flotte, K. Gregory, C. A. Pufialito, and J. G. Fujimoto, "Optical coherence tomography," *Science*, Vol. 254, No. 5035, 1178–1181, 1991.
2. Hitzenberger, C. K. and A. F. Fercher, "Differential phase contrast in optical coherence tomography," *Opt. Lett.*, Vol. 24, No. 9, 622–624, 1999.
3. Sticker, M., C. K. Hitzenberger, R. Leitgeb, and A. F. Fercher, "Quantitative differential phase measurement and imaging in transparent and turbid media by optical coherence tomography," *Opt. Lett.*, Vol. 26, No. 8, 518–520, 2001.
4. Davé, D. P. and T. E. Milner, "Optical low-coherence reflectometer for differential phase measurement," *Opt. Lett.*, Vol. 25, No. 4, 227–229, 2000.
5. Akkın, T., D. P. Davé, T. E. Milner, and H. G. R. III, "Interferometric fiber-based optical biosensor to measure ultra-small changes in refractive index," *Proc. of SPIE*, Vol. 4616, 9–13, 2002.
6. Sticker, M., M. Pircher, E. Gotzinger, H. Sattmann, A. F. Fercher, and C. K. Hitzenberger, "En face imaging of single cell layers by differential phase-contrast optical coherence microscopy," *Opt. Lett.*, Vol. 27, No. 13, 1126–1128, 2002.
7. Fang-Yen, C., M. C. Chu, H. S. Seung, R. R. Dasari, and M. S. Feld, "Noncontact measurement of nerve displacement during action potential with a dual-beam low-coherence interferometer," *Opt. Lett.*, Vol. 29, No. 17, 2028–2030, 2004.
8. Saruni, M. V., S. Weinberg, and J. A. Izatt, "Full-field swept-source phase microscopy," *Opt. Lett.*, Vol. 31, No. 10, 1462–1464, 2006.
9. Choma, M. A., A. K. Ellerbee, C. Yang, T. L. Creazzo, and J. A. Izatt, "Spectral-domain phase microscopy," *Opt. Lett.*, Vol. 30, No. 10, 1162–1164, 2005.
10. Adler, D. C., R. Huber, and J. G. Fujimoto, "Phase-sensitive optical coherence tomography at up to 370,000 lines per second

using buffered Fourier domain mode-locked lasers," *Opt. Lett.*, Vol. 32, No. 6, 626–628, 2007.

11. Joo, C., T. Akkin, B. Cense, B. H. Park, and J. F. de Boer, "Spectral-domain optical coherence phase microscopy for quantitative phase-contrast imaging," *Opt. Lett.*, Vol. 30, No. 16, 2131–2133, 2005.
12. Bachmann, A. H., R. Michaely, T. Lasser, and R. A. Leitgeb, "Dual beam heterodyne Fourier domain optical coherence tomography," *Opt. Express*, Vol. 15, No. 15, 9254–9266, 2007.
13. Zhang, J., B. Rao, L. Yu, and Z. Chen, "High-dynamic-range quantitative phase imaing with spectral domain phase microscopy," *Opt. Lett.*, Vol. 34, No. 21, 3442–3444, 2009.
14. Zainud-Deen, S. H., W. M. Hassen, E. El deen Ali, and K. H. Awadalla, "Breast cancer detection using a hybrid finite difference frequency domain and particle swarm optimization techniques," *Progress In Electromagnetics Research B*, Vol. 3, 35–46, 2008.
15. Rezaiesarlak, R., F. Hodjat Kashani, and E. Mehrshahi, "Analysis of capasitively coupled microstrip-ring resonator based on spectral domain method," *Progress In Electromagnetics Research Letters*, Vol. 3, 25–33, 2008.
16. Tearney, G. J., B. E. Bouma, and J. G. Fujimoto, "High-speed phase- and group-delay scanning with a grating-based phase control delay line," *Opt. Lett.*, Vol. 22, No. 23, 1811–1813, 1997.
17. Wojtkowski, M., A. Kowalczyk, R. Leitgeb, and A. F. Fercher, "Full range complex spectral optical coherence tomography technique in eye imaging," *Opt. Lett.*, Vol. 27, No. 16, 1415–1417, 2002.
18. Hayasaki, Y., "Holographic femtosecond laser processing and three-dimensional recording in biological tissues," *Progress In Electromagnetics Research Letters*, Vol. 2, 115–123, 2008.
19. Izatt, J. A., M. D. Kulkami, S. Yazdanfar, J. K. Barton, and A. J. Welch, "In vivo bidirectional color Doppler flow imaging of picoliter blood volumes using optical coherence tomography," *Opt. Lett.*, Vol. 22, No. 18, 1439–1441, 1997.
20. Wu, T., X. Tang, and F. Xiao, "Research on the coherent phase noise of millimeter-wave Doppler radar," *Progress In Electromagnetics Research Letters*, Vol. 5, 23–34, 2008.
21. Niu, J.-X. and X.-L. Zhou, "Analysis of balanced composite right/left handed structure based on different dimensions of complementary split ring resonators," *Progress In Electromagnetics*

Research, PIER 74, 341–351, 2007.

22. Aldirmaz, S. and L. Durak, "Broadband interference excision in spread spectrum communication systems based on short-time fourier transformation," *Progress In Electromagnetics Research B*, Vol. 7, 309–320, 2008.
23. Hee, M. R., D. Huang, E. A. Swanson, and J. G. Fujimoto, "Polarization sensitive low coherence reflectometer for birefringence characterization and ranging," *J. Opt. Soc. Am. B*, Vol. 9, No. 6, 903–908, 1992.
24. De Boer, J. F., T. E. Milner, and J. S. Nelson, "Determination of the depth-resolved Stokes parameters of light backscattered from turbid media by use of polarization-sensitive optical coherence tomography," *Opt. Lett.*, Vol. 24, No. 5, 300–302, 1999.
25. Hitzenberger, C. K., E. Götzinger, M. Sticker, M. Pircher, and A. F. Fercher, "Measurement and imaging of birefringence and optic axis orientation by phase resolved polarization sensitive optical coherence tomography," *Opt. Express*, Vol. 9, No. 13, 780–790, 2001.
26. De Boer, J. F. and T. E. Milner, "Review of polarization sensitive optical coherence tomography and stokes vector determination," *J. Biomed. Opt.*, Vol. 7, No. 3, 359–371, 2002.